The Journal of Experimental Biology 214, 4000-4009

doi:10.1242/jeb.057539

RESEARCH ARTICLE

Rapid contrast gain reduction following motion adaptation

Karin Nordström[1,2,*], Irene Moyer de Miguel[2] and David C. O'Carroll[2]

[1]Department of Neuroscience, Uppsala University, Box 593, 751 24 Uppsala, Sweden and [2]Adelaide Centre for Neuroscience Research, School of Medical Sciences, University of Adelaide, SA 5005, Australia

*Author for correspondence (Karin.nordstrom@neuro.uu.se)

Accepted 22 August 2011

SUMMARY

Neural and sensory systems adapt to prolonged stimulation to allow signaling across broader input ranges than otherwise possible with the limited bandwidth of single neurons and receptors. In the visual system, adaptation takes place at every stage of processing, from the photoreceptors that adapt to prevailing luminance conditions, to higher-order motion-sensitive neurons that adapt to prolonged exposure to motion. Recent experiments using dynamic, fluctuating visual stimuli indicate that adaptation operates on a time scale similar to that of the response itself. Further work from our own laboratory has highlighted the role for rapid motion adaptation in reliable encoding of natural image motion. Physiologically, motion adaptation can be broken down into four separate components. It is not clear from the previous studies which of these motion adaptation components are involved in the fast and dynamic response changes. To investigate the adapted response in more detail, we therefore analyzed the effect of motion adaptation using a test–adapt–test protocol with adapting durations ranging from 20 ms to 20 s. Our results underscore the very rapid rate of motion adaptation, suggesting that under free flight, visual motion-sensitive neurons continuously adapt to the changing scenery. This might help explain recent observations of strong invariance in the response to natural scenes with highly variable contrast and image structure.

Supplementary material available online at http://jeb.biologists.org/cgi/content/full/214/23/4000/DC1

Key words: motion vision, fast adaptation, time course, flicker, elementary motion detector, EMD.

INTRODUCTION

Neural and sensory systems adapt to prolonged stimulation, thereby optimizing sensitivity to novel stimuli. In the visual pathways, adaptation takes place at all stages: from the photoreceptors themselves, through several post-receptor stages (e.g. Kim and Rieke, 2001; Laughlin, 1989; Rieke and Rudd, 2009; Smirnakis et al., 1997), to higher-order motion-sensitive visual neurons in the brain (e.g. de Ruyter van Steveninck et al., 1986; Kohn and Movshon, 2003; Maddess and Laughlin, 1985; Solomon et al., 2004). Psychophysically, adaptation to prolonged motion stimulation includes the classic 'waterfall effect' for human observers (e.g. Clifford and Ibbotson, 2002). Motion adaptation has been studied extensively in the vertebrate visual cortex, as well as in fly lobula plate tangential cells (LPTCs) (e.g. Kohn and Movshon, 2003; Kurtz et al., 2000; Maddess and Laughlin, 1985; Price et al., 2006; Reisenman et al., 2003). Direction-selective LPTCs are readily identified based on their physiological response properties, allowing data to be pooled from recordings in different animals, thus enabling us to quantify motion vision in more detail than possible in cortical recordings. Importantly, several studies support similar mechanisms underlying motion adaptation in flies and vertebrates (e.g. Clifford and Langley, 1996), making insects an excellent model system for quantifying the underlying neuronal processes.

Motion adaptation can be broken down into four separate components (Harris et al., 2000; Kohn and Movshon, 2003; Nordström and O'Carroll, 2009): (1) a non-directional contrast gain reduction, (2) an antagonistic (direction-selective) after-potential, (3) a non-directional output range reduction and (4) a direction-selective alternating current (AC) component. The after-potential and the AC component have a global effect in adapted neurons, by transferring to previously unstimulated parts of the receptive field (Nordström and O'Carroll, 2009). The contrast gain reduction and the output range reduction, however, are local and do not transfer to previously unstimulated parts of a neuron's receptive field.

Several recent studies have investigated the origin of motion adaptation, the dependence of intracellular calcium levels on adaptation, and to what extent adaptation improves information transmission (e.g. Clifford and Ibbotson, 2002; Fairhall et al., 2001; Kalb et al., 2008; Kurtz et al., 2000; Safran et al., 2007; Solomon et al., 2004). Although many of these studies look at the effects following several seconds of adaptation, more recent experiments using dynamic, fluctuating visual stimuli suggest that adaptation operates on the time scale of the core response of the elementary motion detector (EMD), and thus is likely to be an integral part of it (Borst et al., 2005; Wark et al., 2007). Furthermore, recent work from our own laboratory has highlighted the role of rapid motion adaptation in reliable encoding of the velocity of natural images (Barnett et al., 2010; Straw et al., 2008). However, it is not clear from previous work which motion adaptation components are involved in the fast and dynamic response changes. In this paper, we use a test–adapt–test protocol, which has previously been shown to be a powerful tool for dissociating the key components of adaptation (Harris et al., 2000). By varying the duration of the adapter over a large range, from 20 ms to 20 s, we are able to quantify, for the first time, the time course of each component. Our results underscore the speed at which adaptation operates, suggesting that under free flight the neurons are continuously adapting to the

changing scenery. This might help explain recent observations of strong invariance in the response to natural scenes with highly variable contrast and image structure (Barnett et al., 2010; Straw et al., 2008).

MATERIALS AND METHODS

Electrophysiology

Hoverflies (*Eristalis* sp. Latreille 1804) were caught under permit and stored at 4°C. Prior to experiments they were waxed down with the head tilted forward to gain access to the posterior head surface. We cut a small hole over the left lobula complex and recorded intracellularly from horizontal system (HS) neurons using aluminosilicate electrodes pulled on a Sutter P-97 electrode puller (Novato, CA, USA). The electrodes were filled with 2 mol l^{-1} KCl and had a typical tip resistance of 50–150 MΩ. All experiments were carried out at 24–28°C.

Visual stimuli

The flies were mounted in front of an RGB CRT monitor with a refresh rate of 200 Hz, a mean luminance of 100 Cd m^{-2} and a spatial resolution of 640×480 pixels. We displayed full-screen sinusoidal gratings using a test–adapt–test protocol [adapted from Harris et al. (Harris et al., 2000)]. During 1 s test phases the grating moved in the preferred direction at a near-optimal combination of spatial and temporal frequency (0.1 cycles deg^{-1}, 5 Hz). We then varied the contrast of the test grating to determine the full contrast response function, before and after adaptation. During the adapting phase, the grating moved in the anti-preferred direction for variable durations at a temporal frequency of 20 Hz. As our monitor had a refresh rate of 200 Hz, the shortest adapting duration we could confidently use as a motion stimulus was 20 ms (i.e. four frames). Because of time constraints using intracellular recordings, we used 20 s as the longest adapting duration. We included a minimum 2 s rest between the first test and the adapting stimulus, and a minimum 6 s rest between trials.

As control, we investigated the effect of adapting with flicker stimuli at 20 Hz displayed for 50 ms to 1 s. At 20 Hz, 50 ms corresponds to one full flicker cycle. We adapted with whole-field flicker, or with counter-phase grating flicker (0.1 cycles deg^{-1}), as indicated in the text.

Data analysis

Data were digitized at 5 kHz using a National Instruments 16 bit A/D converter (Austin, TX, USA) and analyzed offline with MATLAB (MathWorks, Natick, MA, USA). We averaged the response measured between 100 and 300 ms following stimulus onset (Harris et al., 2000) after removing the spikelets from the underlying generator potential (Nordström and O'Carroll, 2009). In all analyses we averaged one to five trials within one neuron, before averaging across neurons in different animals. We fitted a Weibull function (Eqn 1) to the contrast sensitivity function to determine C_{50}, defined as the contrast that generates a 50% maximum response in the unadapted neuron:

$$f(x) = \text{offset} + \text{gain}[1 - e^{-(x/\alpha)^{\beta}}], \quad (1)$$

where x is the contrast of the stimulus, α defines the threshold and β the slope of the curve.

To quantify the after-potential we measured the response to a blank screen of mean luminance, following adaptation. By subtracting the after-potential from the adapted response, we normalized the adapted response (Harris et al., 2000). To quantify the output range reduction, we divided the normalized response to a test contrast of 1.0 by the unadapted response to the same test contrast. To quantify the AC component, we performed a fast Fourier transform (FFT) of the raw data (before spikelet removal) and quantified the mean power spectral density between 70 and 110 Hz (see Nordström and O'Carroll, 2009). All these analyses were performed within a 100–300 ms time window post test-stimulus onset.

To identify the earliest possible time window for response analysis, we defined a threshold based on the standard deviation of the response fluctuation in the unstimulated neuron (the mean standard deviation of the membrane fluctuation for 2 s before the start of test 1). We then identified the time point at which the averaged response (N=19) to a test contrast of 1 passed the threshold, as a measure of absolute response latency. We tested in both the preferred and anti-preferred direction and subtracted the responses from each other (i.e. PNP–NNN, where P is preferred and N is null) to avoid measuring the bleed-over response to the adaptor. We quantified the adapted and unadapted responses for 50 and 100 ms immediately following the absolute response latency, for each individual neuron, as above. We normalized the subtracted data to the gain (Eqn 1) of the unadapted contrast response function.

We analyzed all data statistically using GraphPad Prism software (La Jolla, CA, USA), with two-way ANOVAs, followed by paired t-tests (as indicated) with significance allocated to P<0.05 (after Bonferroni correction, where necessary). All data are displayed as means ± s.e.m., unless otherwise stated, where N represents the number of neurons and n the total number of trials.

Model

We implemented a mildly elaborated Hassenstein–Reichardt model in MATLAB. This used an inter-receptor angle of $\Delta\varphi$=1.1 deg, a physiologically realistic value for the separation of frontally orientated EMDs in *Eristalis* (Straw et al., 2006). Spatial pre-filtering was implemented as a two-dimensional Gaussian blur, with $\Delta\rho$=1.4 deg, which approximates the acceptance function of typical fly photoreceptors (Dror et al., 2001; Hardie, 1985). Temporal pre-filtering was implemented by convolution of the local luminance signal with a kernel based on the first-order kernels (impulse response) derived for *Eristalis* lamina monopolar cells (LMCs) using continuously varying white noise stimuli (James, 1990). These kernels can be modeled as the weighted difference of two log-normal functions with different time constants (James, 1990):

$$h(t) = a_1 \exp\{-[\log(t / t_{p1})]^2 / 2\sigma_1^2\} - a_2 \exp\{-[\log(t / t_{p2})]^2 / 2\sigma_2^2\}, \quad (2)$$

where a_1 and a_2 are the weights of the positive and negative terms (1.06 and 0.167, respectively), t_{p1} and t_{p2} are the times to peak (10.1 and 17.5 ms, respectively), and σ_1 and σ_2 (0.197 and 0.395, respectively) are dimensionless shape parameters that determine the curve's width (Dror et al., 2001; Payne and Howard, 1981). The EMD delay was implemented as a first-order low-pass filter with a time constant of 31 ms. Finally, we included a soft (hyperbolic tangent) output saturation with variable gain (Dror et al., 2000), which was non-linearly optimized (using a simplex search algorithm) so that the subtracted (PNP–NNN) model output fit the unadapted contrast sensitivity function measured physiologically.

RESULTS

Test–adapt–test protocol

To investigate the effect of different adapting durations, we used a test–adapt–test protocol (Fig. 1) where we quantified the contrast response function to full-screen sinusoidal gratings before and after adapting hoverfly HS neurons in the anti-preferred direction, thus allowing us to separate the different components of motion

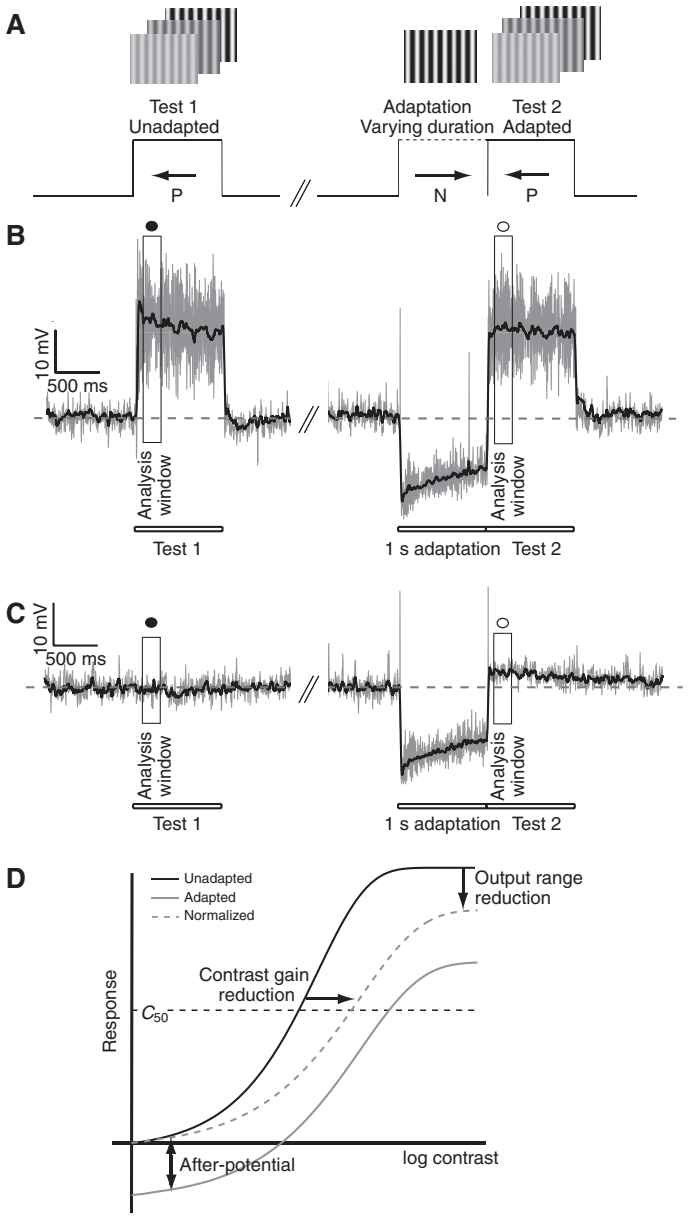

Fig. 1. The test–adapt–test protocol. (A) To investigate the effect of varying the adapting duration, we used a test–adapt–test protocol where we varied the duration of a full-screen sinusoidal adaptor (anti-preferred direction, 0.1 cycles deg^{-1}, 20 Hz). The full-screen test grating (0.1 cycles deg^{-1}, 5 Hz) was displayed for 1.0 s with the contrast varied logarithmically between 0.01 and 1.0. We included a minimum 2 s rest between the first test and the adapting pattern. P, preferred direction of motion; N, anti-preferred (null) direction of motion. (B) The gray data trace show the raw response of a horizontal system (HS) cell to a high-contrast test pattern. Many spikelets ride on the strong depolarization. The black trace shows the filtered average response across three trials after removing the spikelets. The 200 ms analysis time windows (100–300 ms) are boxed (filled circle, unadapted response; open circle, adapted response). (C) The response of the same HS neuron to a test contrast of 0. The after-potential is obvious following adaptation (test 2). (D) Three of the components of motion adaptation (Harris et al., 2000). Contrast gain reduction gives a rightward shift of the adapted contrast response function. Output range reduction gives a compression of the response to high-contrast stimuli in the adapted neuron. The antagonistic after-potential gives a vertical shift of the contrast sensitivity function (up or down).

adaptation (Fig. 1D) (see Harris et al., 2000; Nordström and O'Carroll, 2009). HS neurons respond to high-contrast gratings in a direction-selective manner, depolarizing in the preferred direction (P, tests 1 and 2; Fig. 1A,B) and hyperpolarizing to motion in the opposite direction (N, adaptation). Small depolarizing monophasic events, called spikelets, ride on top of the graded response. The role of spikelets in neural coding is not completely established, but they likely increase the dynamic range of information transmission (Beckers et al., 2007; Beckers et al., 2009; Haag and Borst, 1996; Haag and Borst, 1998). As spikelets are monophasic depolarizing events (Haag and Borst, 1996), they boost the apparent membrane potential. As in our previous study (Nordström and O'Carroll, 2009), we therefore determined the underlying generator potential by removing the spikelets before averaging responses (black trace in Fig. 1B). As previously (Harris et al., 2000; Nordström and O'Carroll, 2009), we measured the response between 100 and 300 ms following stimulus onset (boxed in Fig. 1B).

Four components of motion adaptation

Contrast gain reduction

Following prolonged adaptation in either direction, motion-sensitive neurons showed a pronounced contrast gain reduction (Harris et al., 2000; Kohn and Movshon, 2003) evident by a rightward shift of the contrast response function in the adapted neuron (Fig. 1D). Fig. 2 shows the full contrast response functions before (filled symbols) and after adaptation in the anti-preferred direction (open symbols) for durations ranging from 20 ms to 20 s. Interestingly, we see evidence of substantial contrast gain reduction following even very brief adapting durations (Fig. 2B–D). The unadapted responses represent the response to test 1 for each trial, and thus serve as an internal control to ensure that the adaptation level of the neuron is reset between trials. The contrast gain reduction after the shortest adapting durations is not a residual response to the first test grating, as the unadapted and adapted contrast sensitivity functions overlie each other perfectly in the control, where the adapting duration was 0 s (Fig. 2A).

By subtracting the after-potential (measured as the adapted response to a zero contrast test pattern, i.e. a blank mid-luminance screen; see Fig. 1C,D) we normalized the data (dashed lines in Fig. 2). The after-potential was relatively small after adapting in the anti-preferred direction [see e.g. Harris et al. (Harris et al., 2000), Kurtz (Kurtz, 2007) and Nordström and O'Carroll (Nordström and O'Carroll, 2009) for longer adapting durations] and the normalized data also show a substantial contrast gain reduction after these short adapting durations (Fig. 2B–D). We quantified the contrast gain reduction by measuring C_{50} (Fig. 3A), defined as the contrast needed to generate a 50% maximum response in the unadapted neuron after fitting a Weibull function to the data. The contrast gain reduction increased with adapting duration (Fig. 2E–H, Fig. 3A), reaching a plateau after adapting for several seconds (Fig. 2I–L, Fig. 3A). Increasing the adapting duration further therefore seemed to have little additional effect on the contrast gain reduction. The adapted responses were significantly different from the unadapted responses for each adapting duration (paired t-tests, $P<0.05$; Fig. 3A).

The antagonistic after-potential

Following several seconds of stimulation, visual neurons displayed an antagonistic (direction-selective) after-potential, also called a motion after-effect, which lasted longer and was more pronounced following motion in the preferred direction (Harris et al., 2000; Kurtz et al., 2000). When we used a test contrast of 0 (Fig. 1C) the after-potential was evident in the raw data following 1 s of anti-preferred

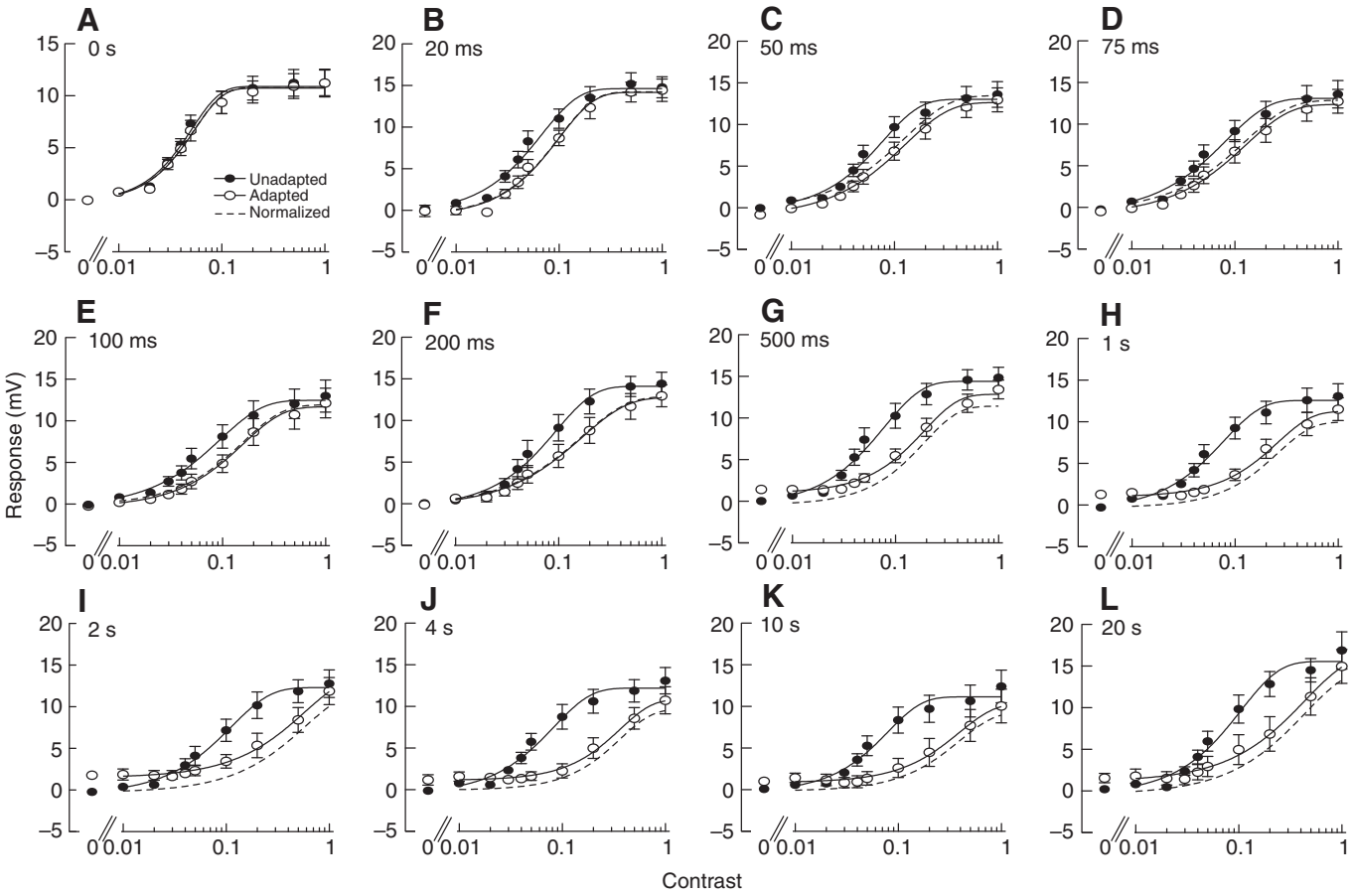

Fig. 2. Contrast sensitivity functions for different adapting durations, before (solid circles) and after (open circles): (A) 0 s adaptation (N=7 neurons, n=18 trials); (B) 20 ms adaptation (N=7, n=17); (C) 50 ms adaptation (N=9, n=23); (D) 75 ms adaptation (N=6, n=18); (E) 100 ms adaptation (N=8, n=21); (F) 200 ms adaptation (N=7, n=17); (G) 500 ms adaptation (N=7, n=18); (H) 1 s adaptation (N=9, n=24); (I) 2 s adaptation (N=7, n=18); (J) 4 s adaptation (N=8, n=23); (K) 10 s adaptation (N=7, n=21); and (L) 20 s adaptation (N=6, n=16). All data are displayed as means ± s.e.m. The dashed lines show the normalized response (generated by subtracting the adapted response to a test contrast of 0 from the remaining adapted responses). In A, the two curves overlap each other perfectly, indicating that the minimum 2 s rest between the first test and the adapting period is sufficient.

direction adaptation. As it is direction selective, the after-potential is manifested as a vertical shift in either direction (up or down) in the contrast response function (Fig. 1D).

To determine the effect of the adapting duration on the after-potential, we measured the adapted response to the zero-contrast test stimulus following each adapting duration (Fig. 1C). Our data (Fig. 3B) show a small antagonistic after-potential after ≥500 ms of anti-preferred adaptation, which remains at a fairly constant level with increasing durations [0.5–20 s, mean 1.37 mV; Fig. 3B; consistent with our earlier work (Harris et al., 2000; Nordström and O'Carroll, 2009)]. There was no significant difference between the after-potential following adapting durations of 0.5–20 s, consistent with an earlier study that found no increased after-potential when using anti-preferred direction adaptation durations of 200 ms to 4 s (Kurtz et al., 2000). However, the after-potential following preferred direction adaptation increased with the adapting duration (Kurtz et al., 2000) (see also supplementary material Fig. S1). Other work (Harris et al., 2000) showed that the strength of the after-potential is proportional to the strength of the response during stimulation.

Output range reduction

Adaptation for several seconds in either direction is followed by an output range reduction (Harris et al., 2000; Kohn and Movshon, 2003), which generates a compression of the contrast sensitivity function to high-contrast stimuli (Fig. 1D). To determine the effect of the adapting duration on the output range reduction, we measured the responses to a test contrast of 1.0 and divided the normalized response (adapted – after-potential) by the unadapted response. As control we measured the output range reduction after 0 s adaptation, which predicatively has a value close to 1 (0 s adapting duration; Fig. 3C). The output range reduction reached a value significantly different than this control, following adaption for 500 ms or more (stars, Fig. 3C). The output range reduction reached a plateau after adapting for several seconds of adaptation, with longer durations having no additional effect.

AC component

We recently described a new global component of motion adaptation, which is most prominent following several seconds of anti-preferred direction motion (Nordström and O'Carroll, 2009). The AC component boosts adapted responses to low-contrast stimuli by increasing the frequency of spikelets generated in the immediate post-adapting period. The fast sodium currents that cause spikelets lead to an amplification at approximately 100 Hz (Haag and Borst, 1996).

To quantify the AC component after different adapting durations, we measured the power of the response at 70–110 Hz after performing

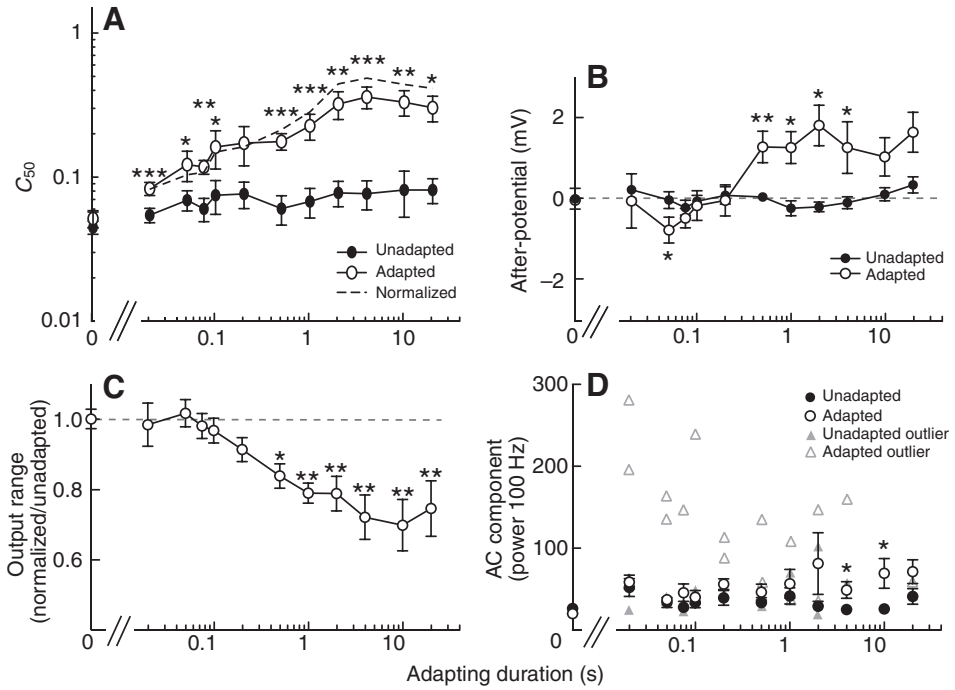

Fig. 3. Motion adaptation components after different adapting durations. (A) Contrast gain reduction quantified by measuring C_{50} in the unadapted (response to test 1, solid circles) and adapted (response to test 2, open circles) neuron. C_{50} was measured as the contrast that gives a 50% maximal response in the unadapted neuron after fitting the data for each neuron in Fig. 2 with a Weibull function (Eqn 1). The dashed line shows C_{50} for the normalized data (without error bars). The adapted and normalized responses are significantly different from the unadapted responses after each adapting duration (paired *t*-tests). (B) After-potential, quantified from the data shown in Fig. 2 by measuring the response to a zero-contrast test grating in the unadapted (response to test 1, solid circles) and adapted (response to test 2, open circles) neuron. Asterisks indicate significant difference between the unadapted and adapted responses for each duration (paired *t*-tests). (C) Output range reduction of the data shown in Fig. 2, quantified by dividing the normalized response to a test contrast of 1.0 by the unadapted response to the same test pattern. Asterisks indicate a significant difference compared with the zero adapting duration (Student's *t*-test, followed by a Bonferroni correction for multiple comparisons). (D) Mean power spectral density of the data in Fig. 2, quantified between 70 and 110 Hz. The solid circles show the data for unadapted neurons, whereas the open circles show the adapted responses. Asterisks indicate a significant difference between the unadapted and adapted response for each duration (paired *t*-tests). Two neurons, which act as outliers in most of the adapted responses, are displayed with gray triangles, and their data are not included in the means. Data in all panels are displayed as means ± s.e.m. (*P<0.05, **P<0.01, ***P<0.001).

a FFT of the raw data (i.e. before removing spikelets) within the same analysis window as before (Fig. 3D). The AC power varies between neurons, and is susceptible to small drifts in the resting membrane potential. In a closer analysis of the individual responses, we noted that two neurons act as outliers (>2×s.d.) following most adapting durations (gray triangles, Fig. 3D). The data for these two neurons were therefore excluded before calculating the means (circles, Fig. 3D). For the remaining neurons, the AC component increased with longer adapting durations.

Adapting with flicker

HS neurons, like other LPTCs, give a strong transient flicker response at the onset and offset of high-contrast visual stimuli (e.g. Borst and Egelhaaf, 1987; Nordström and O'Carroll, 2009). Non-directional flicker stimuli also resulted in reduced contrast sensitivity (i.e. contrast gain reduction) (Harris et al., 2000). Although this effect was weaker than the motion-induced contrast gain reduction, it is possible that flicker-dependent gain reduction represents a contribution of contrast adaptation in earlier stages of visual processing (e.g. in the lamina), which may occur on a different time scale to motion-specific adaptation. To investigate whether the effects following short adapting durations (Fig. 3) may represent a flicker response to the adapting stimulus, we replaced the moving adaptor with a high-contrast, whole-field 20 Hz flicker (1 s adaptation, see Fig. 4A,B). The flicker thus stimulates the eye at the same frequency as the motion adaptor, but with no relative motion cues. During such flicker adaptation, the HS membrane potential is modulated around the resting level (Fig. 4B).

The full contrast sensitivity functions after adapting with flicker at five different durations (50 ms to 1 s) are shown in Fig. 4C–G. Following even the shortest adapting duration (50 ms, Fig. 4C), we see a rightward shift of the curve (contrast gain reduction), which becomes more pronounced after longer adapting durations (Fig. 4F,G). As earlier, we quantified the contrast gain reduction by determining C_{50} in the unadapted and adapted neuron after fitting the data with a Weibull function, and found that flicker induces a significant contrast gain reduction following ≥100 ms adaptation (hashes, Fig. 4H). Earlier work (Harris et al., 2000) showed C_{50} values that were ca. 1.5 times larger following 4 s motion adaptation compared with flicker adaptation, which is consistent with our data (the normalized C_{50} values following anti-preferred motion adaptation are on average 1.7 times larger than following flicker; Fig. 4H; motion data are re-plotted from Fig. 3A for direct comparison).

There is no after-potential after adapting with whole-field flicker (squares, Fig. 4I), consistent with earlier work using 4 s of flicker adaptation (Harris et al., 2000). This differs from adapting with

motion, which induces an after-potential after ≥500 ms anti-preferred adaptation (circles, Fig. 4I; data re-plotted from Fig. 3B).

The output range is not reduced as much following flicker adaptation (average 0.94) as after motion (average 0.91) for adapting durations between 50 ms and 1 s, and is never significantly different from the 0 s adaptation condition (Fig. 4J), consistent with our previous work showing that 4 s of flicker adaptation generates a negligible output range reduction (Harris et al., 2000). Our data (Fig. 4J), and the finding that the output range reduction is more pronounced after adapting with orthogonal motion than with flicker (Harris et al., 2000), suggest that this component is generated after the computation of motion.

There is no consistent difference in the post-adapted AC component following flicker compared with motion adaptation (Fig. 4K). Following flicker adaptation, the mean power spectral density is significantly increased compared with the unadapted response after 100 and 200 ms adaptation, but as there is no consistent trend with increasing adapting durations it is hard to rule out noise in the data.

Early contrast gain reduction

Of the four components of motion adaptation investigated here, the contrast gain reduction appears earliest (Fig. 3). Previous work showed that adaptation operates on varying time scales ranging from tens of milliseconds to several minutes, and that neurons adapt and unadapt on similar time scales (Fairhall et al., 2001; Wark et al., 2007). This suggests that in order to measure the effect following very short adapting durations (e.g. 20 ms) we need to look at the post-adapted response within similar time scales, or the effect might already have disappeared. This is a difficult analysis, however, because the neurons display an absolute response latency of several tens of milliseconds. Therefore, we need to determine the absolute response delay under our experimental conditions. As shown in previous work (Barnett et al., 2010; Warzecha and Egelhaaf, 2000), the response latency increases with decreasing contrast, and the shape of the initial response is highly dependent on the stimulus contrast – whereas high-contrast stimuli display a sharp start-up transient, lower-contrast stimuli build up over several hundred milliseconds (mean responses to test 1 of five different contrasts, N=19, n=240; Fig. 5A).

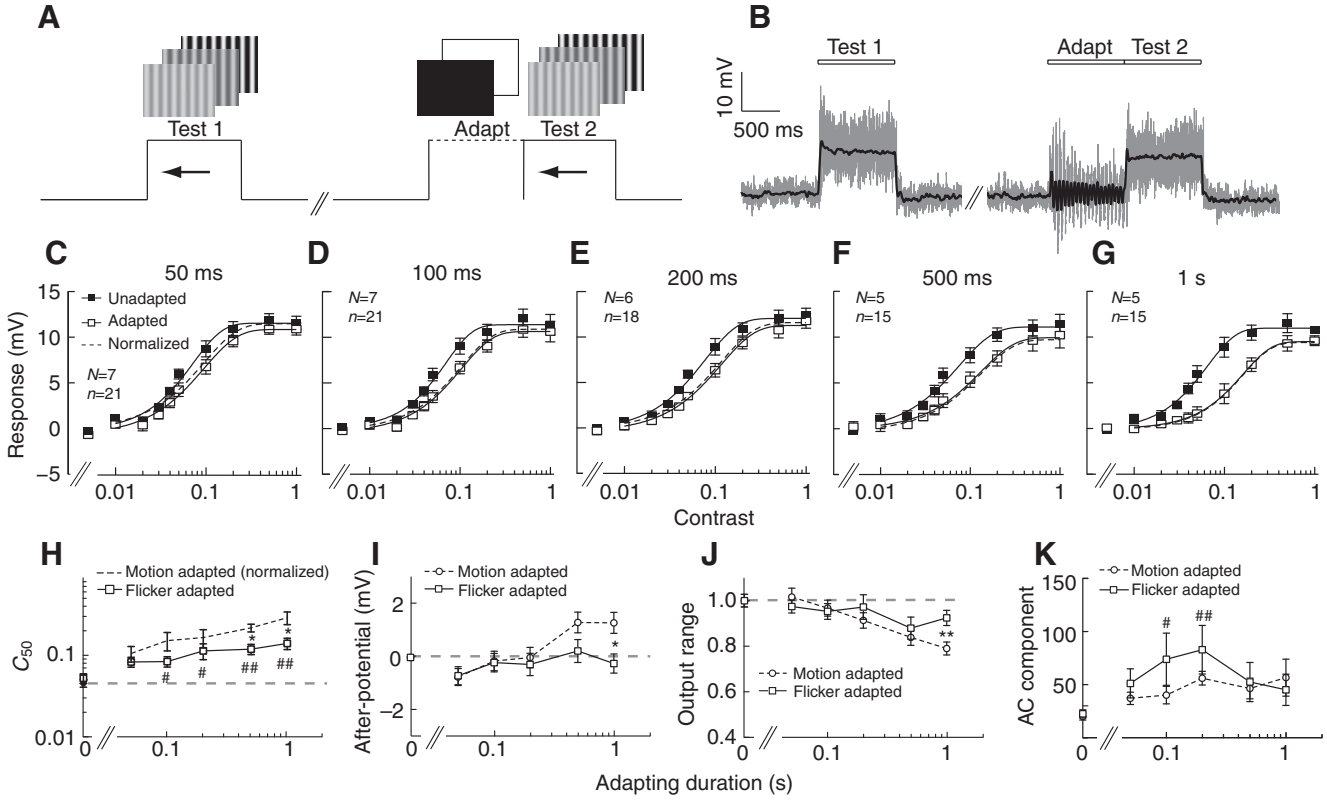

Fig. 4. Adaptation with flicker. (A) To investigate the effect of adapting with flicker we used a test–adapt–test protocol, varying the duration of a whole-field, full-screen flicker adaptor (20 Hz). The full-screen test grating (0.1 cycles deg^{-1}, 5 Hz) was displayed for 1.0 s with the contrast varied logarithmically between 0.01 and 1.0. We included a 2 s rest between the first test and the adapting pattern. (B) The gray data trace shows the raw response of an HS cell to a high-contrast test pattern. The black trace shows the average response across three trials after removing the spikelets. (C–G) Contrast sensitivity functions showing the unadapted (solid squares) and adapted response (open squares) after adapting with whole-field flicker for 50 ms to 1 s. The dashed lines show the normalized data. All data are displayed as means ± s.e.m. (H) C_{50} after adaptation with either motion (dashed) or flicker (squares). The adapted responses are significantly different from the unadapted responses at adapting flicker durations ≥100 ms (paired t-test, $^{\#}P$<0.05, $^{\#\#}P$<0.01). Asterisks indicate a significant difference between the adapted responses following motion adaptation compared with flicker (Student's t-test, P<0.05). (I) After-potential after adaptation with either motion (circles) or flicker (squares). Asterisk indicates a significant difference between the adapted responses following motion adaptation compared with flicker adaptation (Student's t-test, P<0.05). (J) Relative output range reduction (quantified by dividing the normalized response to a test contrast of 1.0 by the unadapted response to the same test pattern) after adaptation with either motion (circles) or flicker (squares). Asterisks indicate a significant difference between the adapted responses following motion adaptation compared with flicker adaptation (Student's t-test, P<0.01). (K) Mean power spectral density (between 70 and 110 Hz) after adaptation with either motion (circles) or flicker (squares). Hashes indicate a significant difference compared with the unadapted response for each duration (paired t-test, $^{\#}P$<0.05, $^{\#\#}P$<0.01). In H–K, the data representing responses after adapting with motion are replotted from Fig. 3.

We identified a threshold response based on the standard deviation of the membrane potential fluctuation in the unstimulated neuron (thin lines, Fig. 5B). In the magnified inset in Fig. 5A, we see that the averaged response to a test contrast of 1.0 passes the standard deviation (i.e. our threshold, thin line in Fig. 5A) 28.3 ms after stimulus onset. The earliest time we can measure the adapted response is thus after ca. 30 ms. However, 30 ms post test-stimulus onset, the generator potential may reflect the response to a brief adapting stimulus, which would also take approximately 30 ms to pass the threshold, rather than reflect the response to the test stimulus currently displayed. To avoid the bleed-over contribution of the response to the adaptor, we subtracted preferred responses from non-preferred direction responses following the same type of adaptation (PPP–NPN or PNP–NNN; Fig. 5B) (and see Barnett et al., 2010). Following such a subtraction, there is still a substantial contrast gain reduction present immediately following the absolute response delay (30–80 ms post-stimulus onset; Fig. 5C). We determined C_{50} as before to quantify the contrast gain reduction (Fig. 5F). As low-contrast stimuli will not have reached the threshold in this 50 ms time window (Fig. 5A), we increased the analysis to 100 ms (30–130 ms post-stimulus onset), and again, found a substantial contrast gain reduction (Fig. 5G). This analysis thus confirms the data shown in Fig. 3A by supporting the presence of motion-induced contrast gain reduction after as little as 20 ms adaptation.

As the contrast gain reduction did not saturate with longer flickering adapting durations and was also weaker after flicker than after motion at all durations (Fig. 4H), it is unlikely to be caused by contrast adaptation in early vision. It could potentially be an inherent effect of the EMD, as flicker stimuli generate a non-directional oscillation due to imbalance in the subtraction mechanism, leading to a weak sensitivity to flicker (Egelhaaf et al., 1989). To investigate the degree to which the very rapid contrast gain reduction (Fig. 5C,F) is an effect of such inherent flicker sensitivity of the EMD, we performed a similar subtraction after adapting with counter-phase flicker (i.e. PFP–NFN) instead of motion (Fig. 5D). As above, this allowed us to tease apart the response to the test stimulus from the bleed-over contribution of the response to the flicker adaptor. The counter-phase flicker stimulus stimulates the underlying EMDs with the same spatial and temporal frequency as the motion adaptor, without providing relative motion cues. Because of spatial lateral inhibition at the inputs to the EMDs, a counter-phase flicker may act as a stronger adaptor than a full-field flicker.

Following such a subtraction, we found that flicker adaptation generated much less contrast gain reduction than motion (Fig. 5D,H). With longer adapting durations, the contrast gain reduction increased (Fig. 5H), consistent with the data shown in Fig. 4H. It is thus unlikely that the rapid contrast gain reduction (Fig. 5C,F,G) is caused by flicker sensitivity generated by the subtraction stage of the EMD; rather, it is more likely to be caused by other mechanisms involved in the computation of motion.

To confirm the conclusion that the rapid contrast gain reduction is not a consequence of intrinsic transient properties of the EMD, we analyzed the output of a mildly elaborated EMD model based on a basic Hassenstein–Reichardt correlator with soft saturation on the output, and mildly elaborated inputs to account for spatiotemporal filtering by the lamina (see Materials and methods). There was no contrast gain reduction after any adapting duration (50 ms adaptation; Fig. 5E), but rather a slight leftward shift of the curve for the shortest adapting durations. In other words, interactions due to the transient nature of the basic EMD led to a weak facilitation of the adapted responses for the shortest adapting durations. Indeed, the possible facilitation resulting from transient interactions within the EMD means that our experiment, if anything, underestimates the reduction in contrast gain for these brief adapting stimuli.

Importantly, if the contrast gain reduction operates on a time scale of tens of milliseconds, this suggests that the unadapted responses measured in Figs 2–3 and in previous work (e.g. Harris et al., 2000; Kurtz et al., 2000) are already themselves adapted. To assess the responses earlier than the 100–300 ms window typically used, however, we have to use a subtraction method as described here (Fig. 5) to avoid measuring the response to the adaptor rather than to the test stimulus. This quickly becomes a prohibitively large experiment, and further, only allows for quantification of the non-directional components, i.e. the contrast gain reduction and the output range reduction. However, from such analysis we see no output range reduction after the shortest adapting durations (Fig. 5C), suggesting that the data for the two non-directional components, shown in Fig. 3, give a fair representation of the underlying adaptation.

DISCUSSION

Few previous studies have looked at the effect of varying the adapting duration. Although some (Kurtz et al., 2000) looked at the strength of the after-potential and the calcium concentration after different adapting durations, they did not investigate the other components of motion adaptation. The formation of after-images and the effects following adaptation with dynamic white noise stimuli have been investigated (Fairhall et al., 2001; Maddess, 1986); however, in these cases the different components of motion adaptation were not dissociated. As very large changes in sensitivity can be masked by saturated responses (e.g. to high-contrast stimuli), quantifying the contrast sensitivity function using a test–adapt–test approach is a powerful method for dissecting the time course of adaptation. To our knowledge this is the first time the four different components of adaptation (Table 1) have been thoroughly quantified following short adapting durations. We show that although contrast gain reduction is extremely rapid, the other three components evolve with similar time scales. All four components saturate after several seconds of stimulation. We also show that flicker sensitivity or other transient properties of the EMD are unlikely to explain the very rapid contrast normalization.

Contrast gain reduction takes place incredibly fast. The effect is non-directional and thus present after adaptation in either the preferred or anti-preferred direction (Harris et al., 2000). The contrast gain reduction is local, in that only those input dendrites directly stimulated by visual motion adapt (Nordström and O'Carroll, 2009), suggesting that it originates pre-synaptic to LPTCs. LPTCs spatially pool information from a large array of EMDs. These input elements to the LPTCs show only weak direction tuning, and the input dendrites serve to both spatially integrate the signal and enhance the direction selectivity (Borst and Haag, 2002; Single et al., 1997). It is possible that the contrast gain reduction is associated with decreased gain at the synaptic input to the LPTCs (see also Nordström and O'Carroll, 2009). Activity-dependent calcium accumulation in LPTCs has previously been linked to some components of adaptation (Dürr and Egelhaaf, 1999; Kurtz, 2007; Kurtz et al., 2000), but this is a relatively slow phenomenon, suggesting that other mechanisms may be responsible for the fastest changes seen here and in previous experiments with dynamic stimuli (Borst et al., 2005; Wark et al., 2007). The other local non-directional component, the output range reduction, is likely caused by other cellular mechanisms than the contrast gain reduction, as it is much slower (Fig. 3C, Table 1).

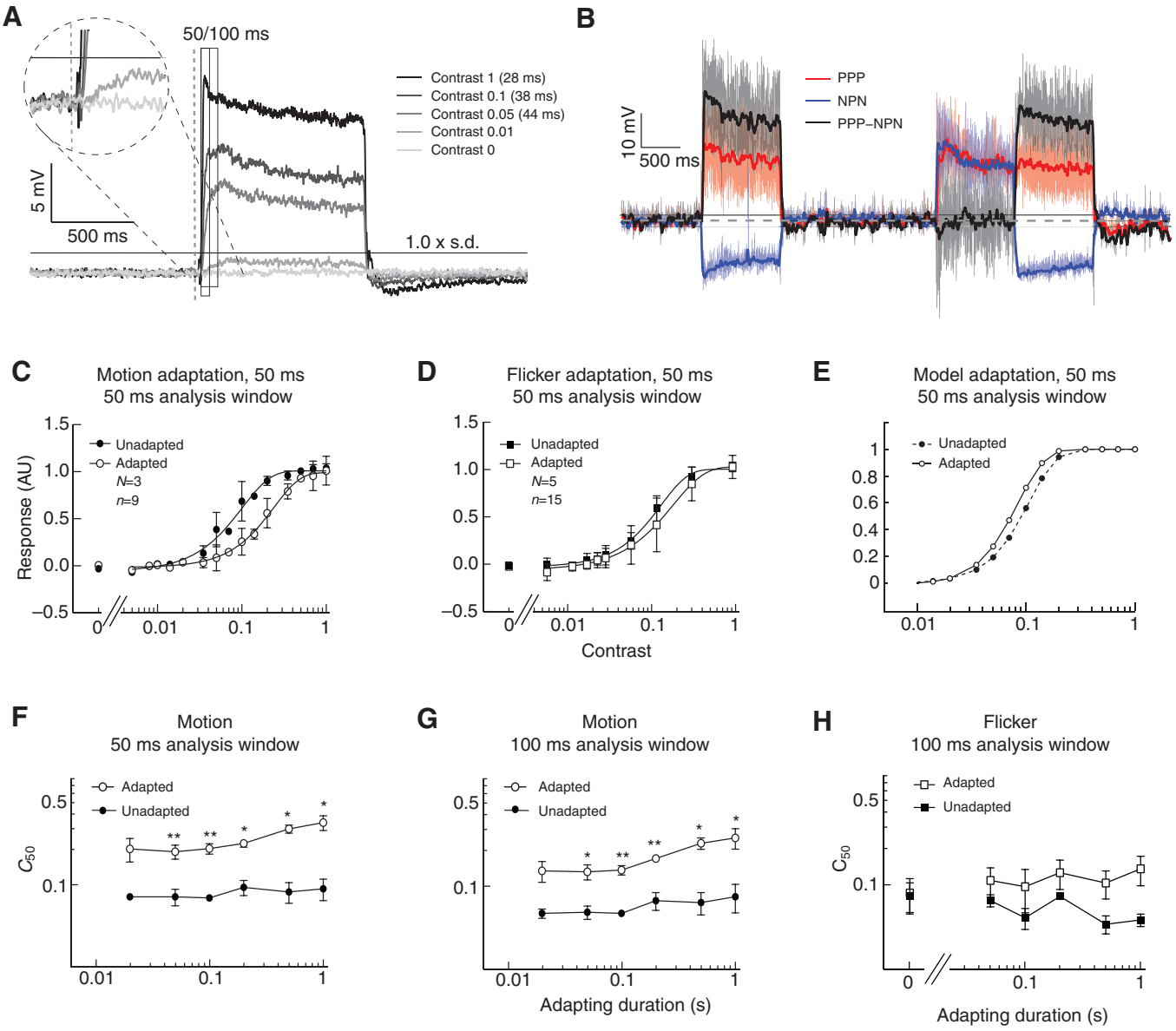

Fig. 5. Contrast gain reduction early in the response. (A) Averaged response to a 1 s preferred direction test stimulus at different contrasts (N=19, n=240). The thin line indicates a 'detectability' criterion based on the standard deviation of the membrane potential in the unstimulated neuron. The gray, dashed vertical line indicates stimulus onset. The magnified inset shows when responses to different test contrasts pass this threshold (see key for delays). The solid darker lines show the same data after removing the spikelets and averaging across three trials. (B) Raw data for 1 s preferred direction adaptation, and preferred direction test (PPP, red) or anti-preferred direction test (NPN, blue). By subtracting NPN from PPP, we minimize the non-directional transient and the bleed-over response to the adaptor (PPP–NPN, gray). The solid darker lines show the same data after removing the spikelets and averaging across three repeats. The dashed line shows 0 (mean membrane potential before stimulus onset) and the thin black lines show the standard deviation of the membrane fluctuation before stimulus onset for this neuron. (C) Contrast response function following motion adaptation for 50 ms, for the subtracted data, within an early time window (30–80 ms post-stimulus onset). (D) Contrast response function following flicker adaptation, for the subtracted data (PFP–NFN) within an early time window (30–80 ms post test-stimulus onset). (E) Output of a mildly elaborated elementary-motion-detector-type correlator model before and after adapting for 50 ms (PNP–NNN, 30–80 ms post-stimulus onset). (F) C_{50} following motion adaptation, measured for the subtracted data within an early time window (30–80 ms post-stimulus onset, N=3, paired t-tests, $^*P$<0.05, $^{**}P$<0.01). (G) C_{50} following motion adaptation, measured for a longer time window (30–130 ms post-stimulus onset, N=3, paired t-tests, $^*P$<0.05, $^{**}P$<0.01). (H) C_{50} for subtracted data (PFP–NFN) following flicker adaptation for the longer time window (30–130 ms post-stimulus onset, N=3 except for 50 ms adaptation where N=5). In C–H, all data are displayed as means ± s.e.m.

We have shown a potent contrast gain reduction on a time scale at least as fast, if not faster, than the 35 ms time constant of the low-pass filter of the EMD, i.e. adaptation is intrinsic to the detection of motion itself. This very rapid contrast normalization (extremely rapid motion-dependent adaptation) on time scales on par with the delay of the EMD provides a partial explanation for the observation that LPTCs display 'velocity constancy' (Straw et al., 2008), whereby the velocity tuning to a range of natural images is very similar despite the images having a large spread of contrasts. This observation has been difficult to reconcile with current models for motion estimation (Barnett et al., 2010; Straw et al., 2008), but if the neurons continuously adapt to the current local contrast on time scales shorter than the low-pass filter of the EMD, this could act to rapidly normalize responses across a

Table 1. Summary of the motion adaptation components

Component	Contrast gain reduction	After-potential	Output range reduction	AC component	Reference
Directionality	Non-directional	Direction selective	Non-directional	Direction selective	Harris et al., 2000; Nordström and O'Carroll, 2009
Spatial spread	Local	Global	Local	Global	Nordström and O'Carroll, 2009
Effect following flicker	Smaller	None	Smaller		Harris et al., 2000; present study
Minimum adapting duration	20 ms	500 ms	500 ms	Seconds	Present study

large range of images. Using dynamic motion stimulation, with velocities that fluctuate rapidly (albeit using white noise rather than natural images), it has been shown that adaptation in LPTCs operates on the same time scale as the response itself (Borst et al., 2005). With increasing velocity fluctuations, the contribution to the response from previous times are suppressed (Borst et al., 2005; Fairhall et al., 2001) so that the system is continuously updating itself to the recent stimulus history.

In fact, during flight, insects are rarely exposed to continuous motion at a single velocity. Rather, they are exposed to a much more dynamic visual stimulus with a large range of spatial frequencies (Tolhurst et al., 1992) and velocities that vary over time (Boeddeker et al., 2005). Measurements of vertebrate eye movement dynamics suggest that these are matched to the substantial variation in local scenes, so that local adaptation builds up and decays rapidly within the time scale of a single fixation (Frazor and Geisler, 2006). Although an efficient coding strategy is to represent those inputs that a neuron typically processes, this becomes difficult when coding natural stimuli that differ greatly on a local scale (both in time and/or space) (Tolhurst et al., 1992) compared with their global distribution. This makes it hard to generate reliable coding, and rapid adaptation dependent on recent stimulus history becomes a prerequisite (Wark et al., 2007). The rapid adaptation we have shown here would no doubt play an important role in this.

LIST OF ABBREVIATIONS

AC	alternating current
EMD	elementary motion detector
HS	horizontal system
LMC	lamina monopolar cell
LPTC	lobula plate tangential cell
NFN	null test, flicker adapt, null test
NNN	null test, null adapt, null test
NPN	null test, preferred adapt, null test
PFP	preferred test, flicker adapt, preferred test
PNP	preferred test, null adapt, preferred test
PPP	preferred test, preferred adapt, preferred test

ACKNOWLEDGEMENTS

We thank the Managers of the Botanic Gardens of Adelaide for allowing us to collect insects and for their ongoing support. We also thank the reviewers whose comments and suggestions greatly improved the manuscript.

FUNDING

This work was funded by the Australian Research Council [grant number DP0880983], US Air Force Office of Scientific Research [grant number FA2386-10-1-4114], Swedish Research Council [grant number 2008-2933], The Royal Swedish Academy of Sciences [grant number FOA10H-119], and P. O. Zetterling Foundation.

REFERENCES

Barnett, P. D., Nordström, K. and O'Carroll, D. C. (2010). Motion adaptation and the velocity coding of natural scenes. *Curr. Biol.* **20**, 994-999.

Beckers, U., Egelhaaf, M. and Kurtz, R. (2007). Synapses in the fly motion-vision pathway: evidence for a broad range of signal amplitudes and dynamics. *J. Neurophysiol.* **97**, 2032-2041.

Beckers, U., Egelhaaf, M. and Kurtz, R. (2009). Precise timing in fly motion vision is mediated by fast components of combined graded and spike signals. *Neuroscience* **160**, 639-650.

Boeddeker, N., Lindemann, J. P., Egelhaaf, M. and Zeil, J. (2005). Responses of blowfly motion-sensitive neurons to reconstructed optic flow along outdoor flight paths. *J. Comp. Physiol. A* **191**, 1143-1155.

Borst, A. and Egelhaaf, M. (1987). Temporal modulation of luminance adapts time constant of fly movement detectors. *Biol. Cybern.* **56**, 209-215.

Borst, A. and Haag, J. (2002). Neural networks in the cockpit of the fly. *J. Comp. Physiol. A* **188**, 419-437.

Borst, A., Flanagin, V. L. and Sompolinsky, H. (2005). Adaptation without parameter change: dynamic gain control in motion detection. *Proc. Natl. Acad. Sci. USA* **102**, 6172-6176.

Clifford, C. W. and Ibbotson, M. R. (2002). Fundamental mechanisms of visual motion detection: models, cells and functions. *Prog. Neurobiol.* **68**, 409-437.

Clifford, C. W. and Langley, K. (1996). Psychophysics of motion adaptation parallels insect electrophysiology. *Curr. Biol.* **6**, 1340-1342.

de Ruyter van Steveninck, R. R., Zaagman, W. H. and Mastebroek, H. A. K. (1986). Adaptation of transient responses of a movement-sensitive neuron in the visual system of the blowfly *Calliphora erythrocephala*. *Biol. Cybern.* **54**, 223-236.

Dror, R. O., O'Carroll, D. C. and Laughlin, S. B. (2000). The role of natural image statistics in biological motion estimation. *Lect. Notes Comput. Sci.* **1811**, 492-501.

Dror, R. O., O'Carroll, D. C. and Laughlin, S. B. (2001). Accuracy of velocity estimation by Reichardt correlators. *J. Opt. Soc. Am. A* **18**, 241-252.

Dürr, V. and Egelhaaf, M. (1999). *In vivo* calcium accumulation in presynaptic and postsynaptic dendrites of visual interneurons. *J. Neurophysiol.* **82**, 3327-3338.

Egelhaaf, M., Borst, A. and Reichardt, W. (1989). Computational structure of a biological motion-detection system as revealed by local detector analysis in the fly's nervous system. *J. Opt. Soc. Am. A* **6**, 1070-1087.

Fairhall, A. L., Lewen, G. D., Bialek, W. and de Ruyter van Steveninck, R. R. (2001). Efficiency and ambiguity in an adaptive neural code. *Nature* **412**, 787-792.

Frazor, R. A. and Geisler, W. S. (2006). Local luminance and contrast in natural images. *Vis. Res.* **46**, 1585-1598.

Haag, J. and Borst, A. (1996). Amplification of high-frequency synaptic inputs by active dendritic membrane processes *Nature* **379**, 639-641.

Haag, J. and Borst, A. (1998). Active membrane properties and signal encoding in graded potential neurons. *J. Neurosci.* **18**, 7972-7986.

Hardie, R. C. (1985). Functional organization of the fly retina. In *Progress in Sensory Physiology*, Vol. 5 (ed. D. Ottoson), pp. 1-80. Berlin: Springer.

Harris, R. A., O'Carroll, D. C. and Laughlin, S. B. (2000). Contrast gain reduction in fly motion adaptation. *Neuron* **28**, 595-606.

James, A. C. (1990). White-noise studies in the fly lamina. PhD thesis, Australian National University, Canberra, Australia.

Kalb, J., Egelhaaf, M. and Kurtz, R. (2008). Adaptation of velocity encoding in synaptically coupled neurons in the fly visual system. *J. Neurosci.* **28**, 9183-9193.

Kim, K. J. and Rieke, F. (2001). Temporal contrast adaptation in the input and output signals of salamander retinal ganglion cells. *J. Neurosci.* **21**, 287-299.

Kohn, A. and Movshon, J. A. (2003). Neuronal adaptation to visual motion in area MT of the macaque. *Neuron* **39**, 681-691.

Kurtz, R. (2007). Direction-selective adaptation in fly visual motion-sensitive neurons is generated by an intrinsic conductance-based mechanism. *Neuroscience* **146**, 573-583.

Kurtz, R., Durr, V. and Egelhaaf, M. (2000). Dendritic calcium accumulation associated with direction-selective adaptation in visual motion-sensitive neurons *in vivo*. *J. Neurophysiol.* **84**, 1914-1923.

Laughlin, S. B. (1989). The role of sensory adaptation in the retina. *J. Exp. Biol.* **146**, 39-62.

Maddess, T. (1986). Afterimage-like effects in the motion-sensitive neuron H1. *Proc. R. Soc. Lond. B* **228**, 433-459.

Maddess, T. and Laughlin, S. B. (1985). Adaptation of the motion-sensitive neuron H1 is generated locally and governed by contrast frequency. *Proc. R. Soc. Lond. B* **225**, 251-275.

Nordström, K. and O'Carroll, D. C. (2009). The motion after-effect: local and global contributions to contrast sensitivity. *Proc. R. Soc. Lond. B* **276**, 1545-1554.

Payne, R. and Howard, J. (1981). Response of an insect photoreceptor-a simple log-normal model. *Nature* **290**, 415-416.

Price, N. S., Crowder, N. A., Hietanen, M. A. and Ibbotson, M. R. (2006). Neurons in V1, V2, and PMLS of cat cortex are speed tuned but not acceleration tuned: the influence of motion adaptation. *J. Neurophysiol.* **95**, 660-673.

Reisenman, C., Haag, J. and Borst, A. (2003). Adaptation of response transients in fly motion vision. I: experiments. *Vis. Res.* **43**, 1291-1307.

Rieke, F. and Rudd, M. E. (2009). The challenges natural images pose for visual adaptation. *Neuron* **64**, 605-616.

Safran, M. N., Flanagin, V. L., Borst, A. and Sompolinsky, H. (2007). Adaptation and information transmission in fly motion detection. *J. Neurophysiol.* **98**, 3309-3320.
Single, S., Haag, J. and Borst, A. (1997). Dendritic computation of direction selectivity and gain control in visual interneurons. *J. Neurosci.* **17**, 6023-6030.
Smirnakis, S. M., Berry, M. J., Warland, D. K., Bialek, W. and Meister, M. (1997). Adaptation of retinal processing to image contrast and spatial scale. *Nature* **386**, 69-73.
Solomon, S. G., Peirce, J. W., Dhruv, N. T. and Lennie, P. (2004). Profound contrast adaptation early in the visual pathway. *Neuron* **42**, 155-162.
Straw, A. D., Warrant, E. J. and O'Carroll, D. C. (2006). A 'bright zone' in male hoverfly (*Eristalis tenax*) eyes and associated faster motion detection and increased contrast sensitivity. *J. Exp. Biol.* **209**, 4339-4354.
Tolhurst, D., Tadmor, Y. and Chao, T. (1992). Amplitude spectra of natural images. *Ophthalmic Physiol. Opt.* **12**, 229-232.
Wark, B., Lundstrom, B. N. and Fairhall, A. (2007). Sensory adaptation. *Curr. Opin. Neurobiol.* **17**, 423-429.
Warzecha, A.-K. and Egelhaaf, M. (2000). Response latency of a motion-sensitive neuron in the fly visual system: dependence on stimulus parameters and physiological conditions. *Vis. Res.* **40**, 2973-2983.